**ADVANCED
SCIENCE NEWS**
www.advancedsciencenews.com

**ADVANCED
MATERIALS**
www.advmat.de

COMMUNICATION

All-Printed Flexible and Stretchable Electronics

Mohammed G. Mohammed and Rebecca Kramer*

Soft, flexible and stretchable electronics will impact and advance diverse fields including wearables, robotics, and biocompatible implantable devices. Many current examples of flexible and stretchable electronics are one-off prototypes, whereas future implementation will require mass production. However, scalable manufacturing with soft materials still presents many unsolved challenges. In this paper, we propose and demonstrate an additive manufacturing process that produces all-printed flexible and stretchable electronics comprised of soft silicone elastomers and liquid metal. We show that this fully automated approach can be used to create complex conductive geometries on a single printing platform, therefore increasing process scalability and repeatability.

All-printed flexible and stretchable electronics have remained elusive, despite the emergence of diverse additive manufacturing processes. The underlying challenge is rooted in the materials and/or geometries required for flexibility and stretchability. There are three basic approaches to achieving flexibility and/or stretchability in conductive materials: conductive polymer composites, geometrically soft conductors, and conductive liquids.

Conductive polymer composites generally consist of a polymer mixed with a tightly packed conductive material.[1–3] While increasing the volume fraction of the conductive material leads to higher conductivity, it also detrimentally alters the mechanical properties of the composite. Geometrically soft conductors refer to thin rigid conductors patterned into unique wavy and curvy structures to achieve stretchability.[4–7] However, the use of inherently rigid materials ultimately limits the strain of these devices and can lead to the formation of cracks and fractures during long-term use.[8,9]

While we believe that each approach offers its own advantages and disadvantages for specific applications, in this work we take the approach of conductive liquid electronics, which are inherently flexible and stretchable, thus bypassing the mechanical limitations of conductive composites and geometrically soft conductors. One common choice of conductive liquid in recent literature is liquid metal. In particular, eutectic gallium–indium alloy (eGaIn; 78 wt% Ga, 22 wt% In[10]) exhibits favorable properties such as a melting point below room temperature,[11,12] low viscosity, high electric conductivity,[13,14] low toxicity, and self-healing capabilities.[15] Liquid metals have been employed in a variety of applications such as flexible and stretchable antennas,[16–18] interconnects,[19,20] wires,[21] electrodes,[22,23] and sensors.[24–26]

Although gallium–indium alloys have properties that make them desirable for flexible electronics, they can be challenging to process. Gallium–indium alloys spontaneously form a thin oxide layer in the presence of atmospheric oxygen, which is the mechanism behind the liquid's useful capability to form freestanding structures,[27,28] but also produces a high surface tension that makes the liquid incompatible with most standard liquid processing techniques.[13,29] The challenges associated with processing liquid metal have led researchers to seek new methods for patterning the material.[30,31] Several emerging methods include injection into elastomeric microchannels,[32,33] imprinting,[34] masked deposition,[35–37] and direct writing.[38–41] The goal behind all of these approaches is to improve the repeatability and scalability of liquid metal processing.

We have previously demonstrated the ability to create printable liquid metal nanoparticle inks by sonicating bulk liquid metal in a carrier solvent.[42] These inks can be patterned using automated printing processes such as inkjet printing, and are mechanically activated by applying pressure to sinter the nanoparticles. However, small particles are required for inkjet printing, while larger particles contain more liquid metal and require lower pressures to sinter. In this paper, we introduce a liquid metal slurry, which is comprised of densely packed microparticles. We further introduce an automated multimode printing process for flexible and stretchable electronics, which includes extrusion printing of the elastomer layers, spray printing of the liquid metal slurry, and mechanical sintering of the slurry particles, all on the same high-precision printing platform. We mechanically activate (i.e., sinter) the particles at room temperature to create conductive paths via automated tapping of a soft tip against the stage, and have found that very small forces are required to activate the larger liquid metal microparticles. The multimaterial automated printing process demonstrated here is capable of manufacturing flexible and stretchable electronics with extremely complex patterns that are not possible using previously demonstrated fabrication techniques. Furthermore, the electrical resistance of the printed devices is fairly low and comparable to the resistance of similar devices fabricated using bulk liquid metal.

The manufacturing process is shown in **Figure 1**. The process combines soft silicone elastomer printing and liquid metal processing on a single high-precision 3D stage using four additive manufacturing steps: extrusion printing of a base elastomer layer, spray printing of liquid metal slurry, selective activation of an electrical path via stage tapping, and extrusion printing of an encapsulating elastomer layer. The extrusion printed and spray-printed materials are fed to the printer nozzle at a constant flow rate using a syringe pump mounted on the 3D stage. Video S1 (Supporting Information) demonstrates all of the fabrication steps.

Preparing Liquid Metal Ink: Before initiating the printing process, we first synthesize the liquid metal ink, which is the

Dr. M. G. Mohammed, Prof. R. Kramer
School of Mechanical Engineering
Purdue University
585 Purdue Mall, West Lafayette, IN 47907, USA
E-mail: rebeccakramer@purdue.edu
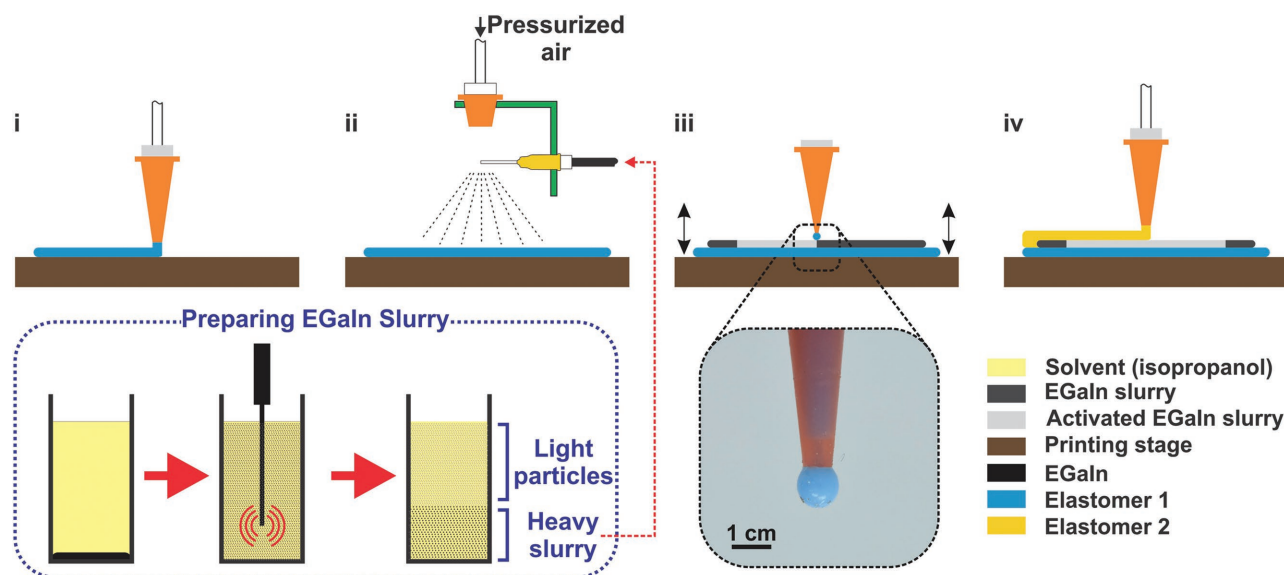
Figure 1. Procedure for printing flexible and stretchable liquid metal electronics: (i) Extrusion printing of a base elastomer layer. (ii) Spray printing of liquid metal slurry. The slurry is produced by sonicating liquid metal in a carrier solvent. (iii) Selective activation of the electrical path by operating the stage in tapping mode against a soft nozzle tip. (iv) Extrusion printing of an encapsulation elastomer to seal the device.

conductive component of the resulting printed electronics. The liquid metal ink we employ is a suspension of liquid metal particles in a carrier solvent achieved via rigorous sonication, as detailed by Hohman, et. al.[43] as well as our previous work.[42] We prepare the liquid metal ink by sonicating 2 g of the bulk liquid metal in 10 mL of isopropanol for 5 min (see Section S1, Supporting Information, for more details about liquid metal ink preparation). An oxide shell spontaneously forms around the particles, which electrically insulates the particles and prevents spontaneous coalescence. Therefore, pressure is required to later sinter the particles by rupturing the oxide shells and merging their liquid cores to create an electrically conductive path, which we refer to as "activation" of the conductive path. In general, large particle films require less pressure to sinter than small particle films.[42] For this reason, we sonicate the liquid metal for only 5 min to produce large particles and further allow the particles to settle under gravity, which separates the ink into a heavy slurry and a suspension of lighter particles in the carrier solvent (see **Figure 2**a). In this work, we employ the liquid metal slurry to ensure easy and reliable particle coalescence in later sintering steps.

Figure 2b shows an example scanning electron microscopy (SEM) image of a deposited particle film, which was analyzed using ImageJ software to determine the distribution of particle sizes in the liquid metal slurry ink. The particle size distribution shows positive skewness around 1 μm, where particles with a diameter greater than 2 μm represent more than 90% of the total mass as shown in Figure 2c. Furthermore, quantitative testing of the pressure required to activate the particle films show that pressures on the order of 1 N mm^{-2} are enough to achieve conductivity across the liquid metal slurry films (see Figure S1, Supporting Information). This agrees with our qualitative observation of the instant conversion of the dull particle film to a conductive shiny liquid film with light pressure using tweezers or a fingertip, as shown in Figure 2d. This "activation

pressure" is a function of the mean particle size, the particle size distribution, and the packing density of the particles.[42] We did not find any detectable correlation between the activation pressure and particle film thickness, as shown in Figure S1d (Supporting Information). With the liquid metal slurry ink synthesized and characterized, we now detail the steps of the printing process.

Extrusion Printing of a Base Elastomer Layer: The base elastomer layer is the foundation on which the liquid metal slurry is printed, activated, and sealed. Therefore, it is crucial to use an elastomer that can be easily printed using the current setup and has no negative impact on subsequent pressure activation or device sealing. We found that very soft elastomers absorb most of the applied pressure during particle sintering, which leads to unachievable or inefficient activation. Therefore, the choice of the base elastomer should be optimized based on the hardness, which impacts activation of the electronics, and elasticity, which contributes to device flexibility and stretchability. After comparing the physical and flow properties of different commercially available elastomers, we chose Smooth-Sil 950 (Smooth-on Inc.) as the base elastomer. The viscosity and pot life of Smooth-Sil 950 allow relatively easy printing with minimal spreading after printing. Moreover, the hardness of cured Smooth-Sil 950 allows easy and efficient activation of the slurry layer printed over it. More details about elastomer choice are available in Section S3 (Supporting Information).

We print the base elastomer layer by feeding the uncured elastomer to a nozzle that is kept at a controlled clearance above the stage and moves horizontally in x and y-directions based on the designed geometry. We can control the thickness of the base layer by manipulating the elastomer flow rate, the stage speed, and the clearance between the nozzle and the stage. The elastomer fully cures in ≈30 min at room temperature and in shorter times by heating the stage. After the elastomer fully cures, liquid metal slurry can be spray printed over it.
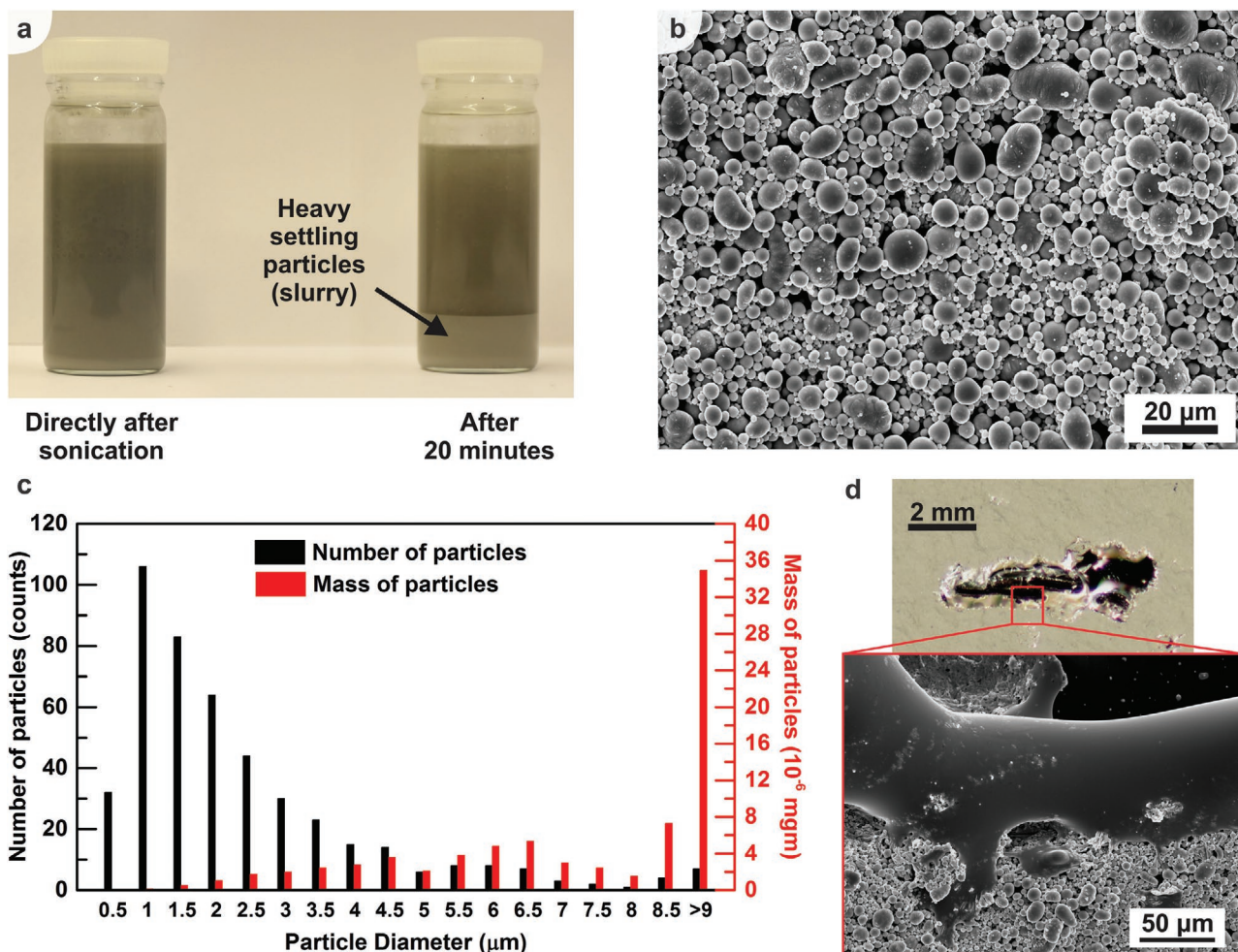
Figure 2. a) Images of liquid metal particles in isopropanol directly after sonication and after 20 min. b) SEM image of a spray-printed film of settled liquid metal particles (slurry). c) Particle size distribution in the liquid metal slurry considering both number and mass of particles. d) Film of liquid metal particles on silicon with a portion partially sintered using tweezers. The inset shows a SEM image of the sintered region.
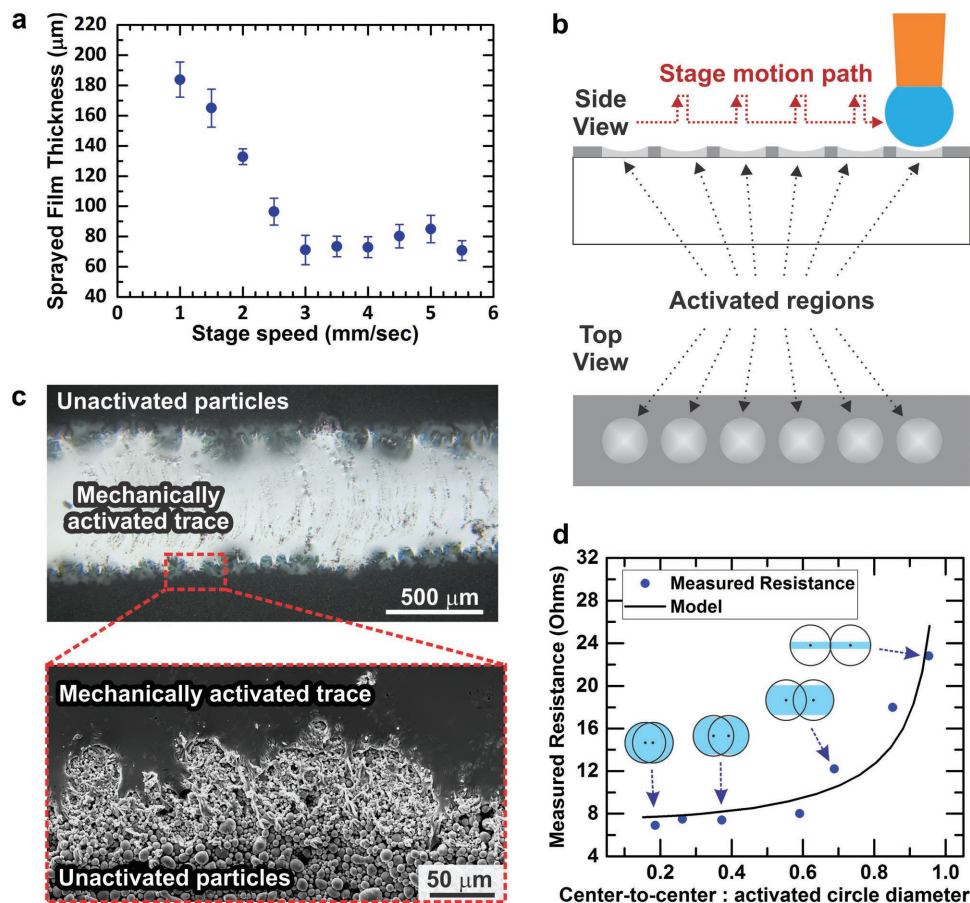
Spray Printing of Liquid Metal Slurry: We initially sought to print the slurry by direct writing using the same setup that was used to extrude elastomer, however the printed films formed cracks when the solvent evaporated as a result of aggregation of particles, which is a common phenomenon in similar drying films.[44,45] Therefore, we used spray printing to achieve consistent and uniform deposition of crack-free films of liquid metal particles. We installed a simple custom-made spray printing nozzle 10 cm above the stage. The slurry is injected into the nozzle and pressurized air is blown perpendicular to the nozzle to spray the slurry on the substrate. Slurry deposition by spray printing is more time efficient than deposition by direct writing, as the slurry covers wider areas in shorter periods of time.

We control the thickness of the printed film by manipulating the stage speed and the flow rate of the slurry. **Figure 3**a shows that the spray-printed film thickness decreases as the speed of the stage increases at constant slurry flow rate. Thicker films may be achieved using higher slurry flow rates or lower stage speeds. A predesigned mask can be used to control the areas covered with the liquid metal slurry, which is ready to activate directly after it is printed.

Selective Activation of the Electrical Path via Stage Tapping: We activate the deposited particle film by operating the stage in a tapping mode, where the stage moves up and down at a set frequency and simultaneously in *x* and *y*-directions. The pressure applied by the nozzle onto the particle film when operating the stage in tapping mode mechanically activates the desired conductive path. The nozzle tip used for activation is a syringe needle with a soft elastomer cap (inset in Figure 1), which results in circular activated areas. The soft cap is necessary to ensure activation without scraping the particles off the substrate. Figure 3b shows the repetitive step motion sequence of the stage relative to the nozzle to form an activated path. Section S4 (Supporting Information) includes more about the tapping mode parameters and their effect on the continuity of the activated trace.

The automated tapping mechanism yields activated traces with rough edges, which can be observed from the optical image in Figure 3c. The optical image also shows texture on the oxide skin formed on the surface of the activated trace. We suspect that the texture is a result of oxide skin wrinkling that takes place during activation, as liquid metal adhesion to the

**ADVANCED
MATERIALS**
www.advmat.de

**ADVANCED
SCIENCE NEWS**
www.advancedsciencenews.com

COMMUNICATION

Figure 3. a) Thickness of spray-printed slurry films as a function of stage speed at a slurry flow rate of 0.2 mL min⁻¹. b) Schematic of stage motion relative to the activation tip during the activation step. c) Optical image of an activated trace. The inset SEM image shows the edge of the trace. d) Resistance of activated traces as a function of the normalized center-to-center distance between activated circles. The schematics on the plot show two consecutive activated circles with the highlighted region representing the effective electrically conductive path.

soft activation tip causes the surface oxide to fracture, reform, and compress during the dynamic process. More details and SEM images of the activated trace surface texture are available in Section S5 (Supporting Information).

The resistance of the continuous trace is determined by the minimum width of that trace, which in our case is the width of the intersecting area between two consecutive activated circles. Figure 3d shows the resistance of activated traces against the normalized center-to-center distance between the activated circles (the ratio between the center-to-center distance and the diameter of the activated area). Note that for ratios greater than 1 the trace is discontinuous and not conductive. The schematics on the plot show two consecutive activated circles with the highlighted region representing the effective electrically conductive path. We developed a simple model alongside the experimental results, which predicts the trace resistance based on the tapping parameters. The resistance R can be calculated from the formula
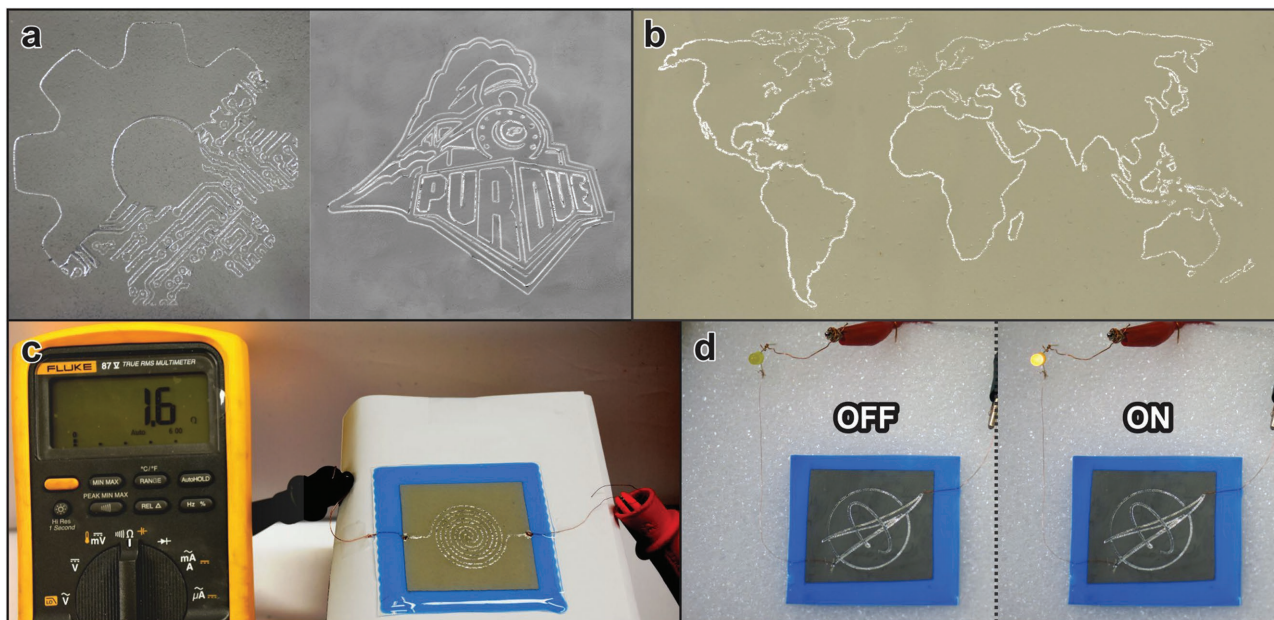
$$R = \frac{\rho L}{A} = \frac{\rho L}{TW} = \frac{\rho L}{T \times 2r \cos\left(\sin^{-1}\left(\frac{d}{2r}\right)\right)} \quad (1)$$

where ρ is the resistivity of eGaIn; A, T, L, and W are the cross-sectional area, thickness, length, and width of the activated

trace, respectively; r is the radius of one activated circle; and d is the center-to-center distance of two successively activated circles. More details about the model and its derivation are available in Section S6 (Supporting Information). The model shows very good agreement with the experimental data and confirms the effect of the center-to-center distance on the resistance of the final activated trace, as shown in Figure 3d.

Extrusion Printing of an Encapsulation Elastomer: The last step in the printing process is sealing the device after connecting wires to the terminals of the activated pattern (see Section S7, Supporting Information). We use Sylgard 184 (Dow Corning) as a sealing elastomer since its relatively low viscosity allows it to infiltrate between the unactivated particles and prevent further activation. It readily bonds with the Smooth-Sil 950 base layer because it is also a silicon-based elastomer. The diffusion of Sylgard-184 through the particles and its strong bonding with Smooth-Sil 950 help the devices to behave as a single unit without any delamination through long-term use.

Figure 4 shows examples of printed functional devices. Figures 4a–b show very complex patterns in the form of the Faboratory lab logo, the Purdue University train, and a world map representation. These patterns are almost impossible to create using previous liquid metal-embedded device fabrication

**ADVANCED
SCIENCE NEWS**

www.advancedsciencenews.com

**ADVANCED
MATERIALS**

www.advmat.de

COMMUNICATION

Figure 4. a–b) Demonstration of fully printed complex geometries: Faboratory gear, Purdue train, and world map. c) Resistance measurement of a printed coil 268 mm long, 500 µm wide, and 90 µm thick. d) NASA logo patterned on eGaIn slurry and acting as an electric circuit.

methods, such as injection into microchannels. The low electric resistivity of liquid metal ($29.4 \times 10{-}6$ Ω cm[13]) makes the resistance of printed circuits using the printing process fairly low; an example is shown in Figure 4c, where the resistance of a seven-turn coil pattern is 1.6 Ω, which is in the same order of magnitude of the resistances of devices with similar dimensions that use bulk liquid metal as the conductive material. Figure 4d shows a printed circuit with a complex geometry (the NASA logo) connected as a part of an electric circuit without affecting the continuity of the circuit.

The printing procedure not only allows printing of functional devices with extremely complex geometries, but also provides the robustness, flexibility, and stretchability inherent to liquid metal-embedded devices (**Figure 5**a). To demonstrate this point, we used the printing process to fabricate sensors based on previously developed designs for liquid metal strain and pressure sensors.[24] Figure 5b shows a pressure sensor that changes resistance as a function of the pressure applied by a fingertip. We also fabricated a strain sensor and measured its output resistance as a function of strain between 0% and 30% for 500 continuous cycles. We found the sensor response to be stable, linear, and similar to the responses of similar sensors made using previous fabrication approaches. Further details about strain sensor testing are available in Section S8 (Supporting Information).

We note that we observed a reduction in the resistance across the printed pressure sensors with long-term use. We hypothesized that this drift was a result of further activation of the particles surrounding the activated trace, which leads to a wider conductive trace and therefore decreased resistance. We confirmed this hypothesis by comparing microscope images of activated paths before and after applying a uniform pressure and found that the width of paths consistently increased by approximately 140 µm (70 µm on each side). For example, the width of an activated path increased from 800 to

940 µm after applying the uniform pressure. Therefore, the signal drift may be avoided by applying substantial and uniform pressure to the sensors prior to use, which coalesces any remaining liquid metal particles near the traces and stabilizes the sensor signal.
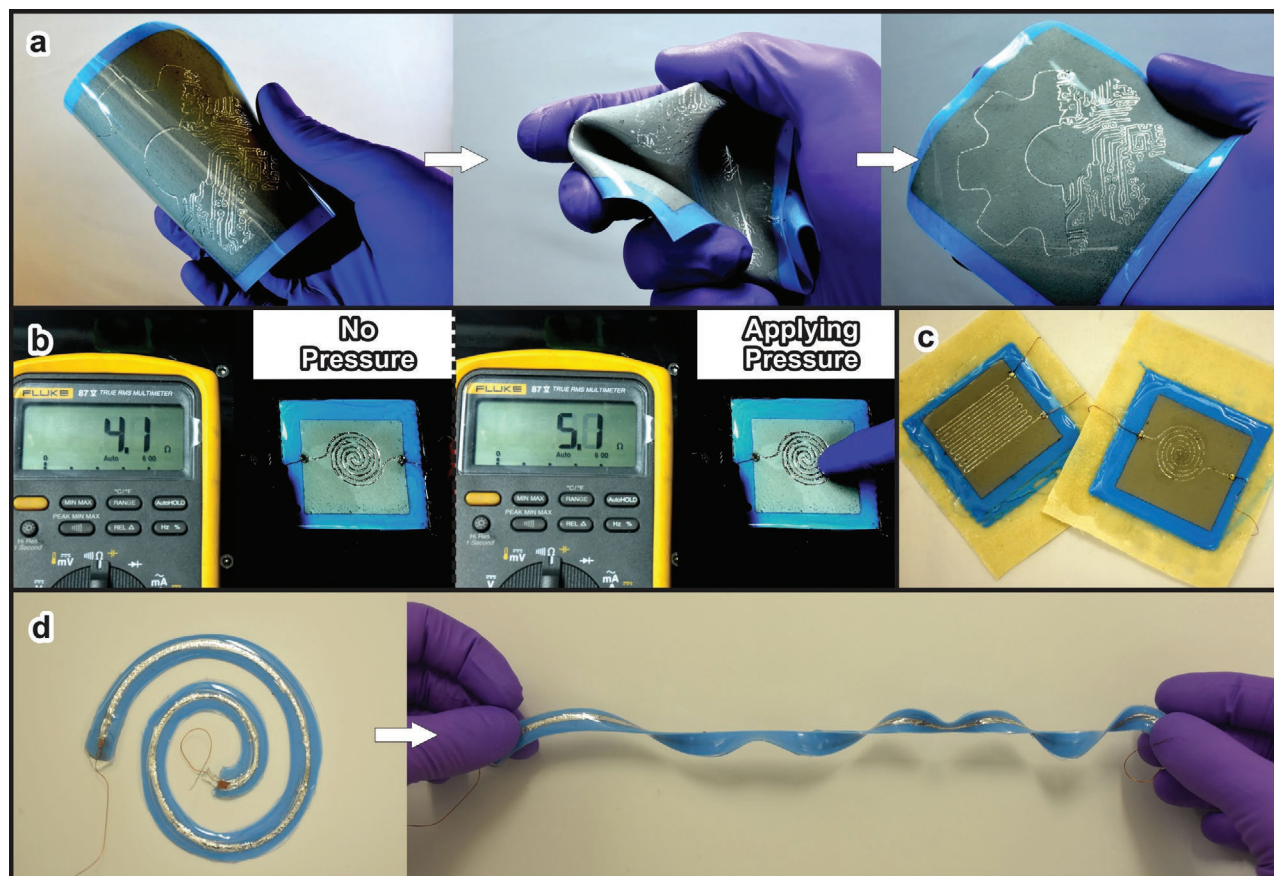
The process described in this paper enables printing functional electronics on different substrates and makes the process compatible with several applications. We show here two examples of potential applications: wearable sensors and stretchable wires.

To demonstrate wearable sensing, we printed strain and pressure sensors onto muslin fabric, as shown in Figure 5c. The base elastomer layer mechanically infiltrates and bonds to the fabric, and the full devices reliably sense strain or pressure. The stretchability of the elastomers used to fabricate these sensors is higher than that of the fabric, resulting in sensory fabrics that will minimally impact the natural range of motion of the wearer in potential wearable electronic applications, relative to wearable systems using rigid and unstretchable components.

To demonstrate stretchable wires, we printed a coil-shaped wire that can be stretched to a straight wire longer than the length of the printing stage, as shown in Figure 5d. It is possible to create longer wires by increasing the number of turns in the coil. The wire maintains its electric conductivity at the coiled and stretched states (Video S2, Supporting Information). Flexible and stretchable conductive wires have been previously used to make stretchable headphones and chargers.[21]

Finally, we evaluate the process reliability and throughput, which are critical for any large-scale production processes. The yield of working fully printed devices is 75% based on 20 samples (sensors, wires, and complex geometry patterns) with a low rate of failure. The main source of device failure is poor interfacing between the copper wire and the activated path (60% of failures), which we discuss in Section S7 (Supporting Information).

**ADVANCED
MATERIALS**
www.advmat.de

**ADVANCED
SCIENCE NEWS**
www.advancedsciencenews.com

COMMUNICATION

Figure 5. a) Demonstration of the printed electronics being bent, squeezed, and released with no electrical or mechanical damage. b) Demonstration of a printed pressure sensor changing resistance in response to applied pressure. The activated trace is 268 mm long, 500 µm wide, and 40 µm thick. c) Pressure and strain sensors printed on fabric. d) A printed wire in both a coiled and stretched position.

The process throughput depends on the time consumed by all involved fabrication steps. For relatively simple geometries, the time needed to print the elastomers, as well as spray print and activate the liquid metal slurry does not exceed 15 min. However, the time required for the elastomers to fully cure makes the actual process take more than 6 h. Heating the stage to 60 °C reduces the elastomers curing time to 2 h and enhances the process throughput.

In conclusion, we have demonstrated a fully automated printing process for liquid metal-based flexible and stretchable electronics. To enable this process, we have constructed a custom multimaterial additive printer that combines multiple printing processes on a single platform. We have demonstrated all-printed flexible and stretchable electronics via extrusion printing of elastomers, spray printing of a liquid metal microparticle ink, and automated liquid metal microparticle sintering enabled by tapping a soft tip against printed particle films. The automation of liquid metal-based electronics enables improvements in device reliability, reproducibility, and throughput. We have demonstrated that the printing process can produce liquid metal-based sensors with a similar design to those already described in the literature. Furthermore, we have shown that this printing process can

produce complex conductive patterns that cannot be achieved by previous and non-automated fabrication approaches. Further optimization of the multimaterial printing process will enable the transition of this technology from the laboratory into commercial applications such as soft robotics, sensor skins, and wearables.

Supporting Information

Supporting Information is available from the Wiley Online Library or from the author.

Acknowledgements

[1] K.-Y. Chun, Y. Oh, J. Rho, J.-H. Ahn, Y.-J. Kim, H. R. Choi, S. Baik, *Nat. Nanotechnol.* **2010**, *5*, 853.

[2] Y.-J. Yang, M.-Y. Cheng, W.-Y. Chang, L.-C. Tsao, S.-A. Yang, W.-P. Shih, F.-Y. Chang, S.-H. Chang, K.-C. Fan, *Sens. Actuators, A* **2008**, *143*, 143.

[3] M. Chen, T. Tao, L. Zhang, W. Gao, C. Li, *Chem. Commun.* **2013**, *49*, 1612.

[4] Y. Sun, W. M. Choi, H. Jiang, Y. Y. Huang, J. A. Rogers, *Nat. Nanotechnol.* **2006**, *1*, 201.

[5] D.-H. Kim, J. A. Rogers, *Adv. Mater.* **2008**, *20*, 4887.

[6] J. Jeong, S. Kim, J. Cho, Y. Hong, *IEEE Electron Device Lett.* **2009**, *30*, 1284.

[7] D.-H. Kim, J. Xiao, J. Song, Y. Huang, J. A. Rogers, *Adv. Mater.* **2010**, *22*, 2108.

[8] Y.-Y. Hsu, B. Dimcic, M. Gonzalez, F. Bossuyt, J. Vanfleteren, I. De Wolf, in *5th Int. Microsystems, Packaging, Assembly and Circuits Technology Conf. IMPACT 2010*, **2010**, pp. 1–4.

[9] F. Bossuyt, J. Guenther, T. Löher, M. Seckel, T. Sterken, J. de Vries, *Microelectron. Reliab.* **2011**, *51*, 628.

[10] T. J. Anderson, I. Ansara, *J. Phase Equilib.* **1991**, *12*, 64.

[11] S. J. French, D. J. Saunders, G. W. Ingle, *J. Phys. Chem.* **1937**, *42*, 265.

[12] W. J. Svirbely, S. M. Selis, *J. Phys. Chem.* **1954**, *58*, 33.

[13] D. Zrnic, D. S. Swatik, *J. Less-Common Met.* **1969**, *18*, 67.

[14] S. Yu, M. Kaviany, *J. Chem. Phys.* **2014**, *140*, 64303.

[15] E. Palleau, S. Reece, S. C. Desai, M. E. Smith, M. D. Dickey, *Adv. Mater.* **2013**, *25*, 1589.

[16] J. So, J. Thelen, A. Qusba, G. J. Hayes, G. Lazzi, M. D. Dickey, *Adv. Funct. Mater.* **2009**, *19*, 3632.

[17] S. Cheng, A. Rydberg, K. Hjort, Z. Wu, *Appl. Phys. Lett.* **2009**, *94*, 144103.

[18] M. Kubo, X. Li, C. Kim, M. Hashimoto, B. J. Wiley, D. Ham, G. M. Whitesides, *Adv. Mater.* **2010**, *22*, 2749.

[19] H.-J. Kim, C. Son, B. Ziaie, *Appl. Phys. Lett.* **2008**, *92*, 11904.

[20] J. Yoon, S. Y. Hong, Y. Lim, S.-J. Lee, G. Zi, J. S. Ha, *Adv. Mater.* **2014**, *26*, 6580.

[21] S. Zhu, J.-H. So, R. L. Mays, S. Desai, W. R. Barnes, B. Pourdeyhimi, M. D. Dickey, *Adv. Funct. Mater.* **2013**, *32*, 2308.

[22] J.-H. So, M. D. Dickey, *Lab Chip* **2011**, *11*, 905.

[23] N. Hallfors, A. Khan, M. D. Dickey, A. M. Taylor, *Lab Chip* **2013**, *13*, 522.

[24] Y.-L. Park, C. Majidi, R. Kramer, P. Bérard, R. J. Wood, *J. Micromech. Microeng.* **2010**, *20*, 125029.

[25] C. Majidi, R. Kramer, R. J. Wood, *Smart Mater. Struct.* **2011**, *20*, 105017.

[26] R. K. Kramer, C. Majidi, R. Sahai, R. J. Wood, in *2011 IEEE/RSJ Int. Conf. Intelligent Robots and Systems, IROS*, **2011**, pp. 1919–1926.

[27] C. Ladd, J.-H. So, J. Muth, M. D. Dickey, *Adv. Mater.* **2013**, *25*, 5081.

[28] C. Trlica, D. P. Parekh, L. Panich, C. Ladd, M. D. Dickey, *Micro- and Nanotechnology Sensors, Systems, and Applications VI*, **2014**, 90831D, Balimore, MD, USA.

[29] S. Cheng, Z. Wu, *Lab Chip* **2012**, *12*, 2782.

[30] M. D. Dickey, *ACS Appl. Mater. Interfaces* **2014**, *6*, 18369.

[31] I. D. Joshipura, H. R. Ayers, C. Majidi, M. D. Dickey, *J. Mater. Chem. C* **2015**, *3*, 3834.

[32] J. Park, S. Wang, M. Li, C. Ahn, J. K. Hyun, D. S. Kim, D. K. Kim, J. A. Rogers, Y. Huang, S. Jeon, *Nat. Commun.* **2012**, *3*, 916.

[33] M. Gao, L. Gui, *Lab Chip* **2014**, *14*, 1866.

[34] B. A. Gozen, A. Tabatabai, O. B. Ozdoganlar, C. Majidi, *Adv. Mater.* **2014**, *26*, 5211.

[35] S. H. Jeong, A. Hagman, K. Hjort, M. Jobs, J. Sundqvist, Z. Wu, *Lab Chip* **2012**, *12*, 4657.

[36] R. K. Kramer, C. Majidi, R. J. Wood, *Adv. Funct. Mater.* **2013**, *23*, 5292.

[37] Q. Zhang, Y. Gao, J. Liu, *Appl. Phys. A* **2013**, *116*, 1091.

[38] Y. Zheng, Z. He, Y. Gao, J. Liu, *Sci. Rep.* **2013**, *3*, 1786.

[39] J. W. Boley, E. L. White, G. T.-C. Chiu, R. K. Kramer, *Adv. Funct. Mater.* **2014**, *24*, 3501.

[40] Y. Zheng, Z.-Z. He, J. Yang, J. Liu, *Sci. Rep.* **2014**, *4*, 4588.

[41] Q. Wang, Y. Yu, J. Yang, J. Liu, *Adv. Mater.* **2015**, *27*, 7109.

[42] J. W. Boley, E. L. White, R. K. Kramer, *Adv. Mater.* **2015**, *27*, 2355.

[43] J. N. Hohman, M. Kim, G. A. Wadsworth, H. R. Bednar, J. Jiang, M. A. LeThai, P. S. Weiss, *Nano Lett.* **2011**, *11*, 5104.

[44] E. A. Jagla, *Phys. Rev. E* **2002**, *65*, 46147.

[45] W. P. Lee, A. F. Routh, *Langmuir* **2004**, *20*, 9885.